Phase-field-crystal model of phase and microstructural stability in driven nanocrystalline systems

Nana Ofori-Opoku,[1,*] Jeffrey J. Hoyt,[1] and Nikolas Provatas[1,2]

[1]*Department of Materials Science and Engineering and Brockhouse Institute for Materials Research, McMaster University, 1280 Main Street West, Hamilton, Canada L8S 4L7*

[2]*Department of Physics and Centre for the Physics of Materials, Rutherford Building, McGill University, 3600 Rue University, Montreal, Canada H3A 2T8*

(Received 18 September 2012; published 21 December 2012)

We present a phase-field-crystal model for driven systems which describes competing effects between thermally activated diffusional processes and those driven by externally imposed ballistic events. The model demonstrates how the mesoscopic Enrique and Bellon [Phys. Rev. Lett. **84**, 2885 (2000)] model of externally induced ballistic mixing can be incorporated into the atomistic phase-field-crystal formalism. The combination of the two approaches results in a model capable of describing the microstructural and compositional evolution of a driven system while incorporating elastoplastic effects. The model is applied to the study of grain growth in nanocrystalline materials subjected to an external driving.

DOI: 10.1103/PhysRevE.86.066706 PACS number(s): 64.70.Nd, 81.30.Bx, 61.72.−y

I. INTRODUCTION

There has been an explosion over the past couple of decades in the investigation of nanocrystalline (NC) materials as viable replacements for components in varying industries, from microelectronics and integrated circuits to core components in nuclear reactors. Due to the small-size features exhibited by NC materials, and their propensity to have a high density of grain boundaries and phase boundaries, the mechanical, chemical, electrical, and optical properties of NC materials differ quite markedly from their polycrystalline counterparts.

Whether for tuning nanostructure-size features in components during their fabrication (microelectronics) or as full-size components in nuclear reactors, the microstructural and phase stability of these components, when exposed to external driving, is paramount. These external processes may be attributed to neutron or electron irradiation (in nuclear systems), ion-beam mixing (in the fabrication of microelectronics), or continued plastic deformation (leading to cyclic fatigue, e.g., high-energy milling) [1]. Of importance in these systems is the structural integrity of components. The system is driven out of equilibrium (as described by thermally activated processes, i.e., thermodynamic equilibrium), and in the thermodynamic limit a system may exhibit chemical or structural modifications manifested in microstructural and phase alterations. The resulting long-time configurations of these systems are then dependent on the conditions responsible for external driving.

For polycrystalline materials, there are several exhaustive reviews and no shortage of literature on materials under external driving conditions, particularly when the forcing condition is a flux of energetic particles (such as electrons, ions, or neutrons) [1–3]. Several interesting and unique phenomena can occur in these materials. Examples include precipitation in undersaturated solid solutions [4], the lowering of the critical point in second-order order-disorder transitions [1,5], the patterning of dislocations [6], and the amorphization of crystalline materials [1,7]. External driving is also usually accompanied by the production of excess point defects, which, among other things, enhance thermal diffusion.

The common denominator in all driven systems is that they achieve an altered dynamical state, where the configuration of such a state is a function of the material properties and forcing conditions [1]. The resulting state can be rationalized as being caused by the long-time effect of two parallel yet competing mechanisms: thermally activated atomic jumps and the forced (athermal ballistic) atomic jumps arising from external forcing. Research suggests that a method to alleviate the effects of these athermal ballistic effects is the use of NC materials, which feature a very high density of potential point-defect sinks such as grain boundaries or interphase boundaries. Recently, Bai *et al.* [8] outlined a theoretical explanation for the apparent resistance of NC materials (pure Cu) to ballistic conditions. This resistance to ballistic effects has also been observed experimentally by Rose and co-workers [9] on NC Pd and ZrO_2 materials, Hochbauer *et al.* [10] on Cu-Nb multilayers, and in various atomistic simulations [11,12]. Unfortunately, most existing atomistic models are not capable of capturing the long-time scales relevant in studying sustained ballistic effects. While techniques have been developed to accelerate atomistic simulations [8], it is not clear if these methods can be extended to a time scale appropriate for the solid-state diffusion mechanisms controlling the microstructural and phase stability of NC materials.

Enrique and Bellon [13,14] recently developed a continuum description of alloys subjected to external driving via ballistic events. The underlying theme of their model is the competition between two dynamical mechanisms: one is thermally driven to bring the system to thermodynamic equilibrium, and the other is athermal particle exchanges driving the system out of equilibrium, an idea which dates back to Martin [15]. This is accomplished through an effective free-energy functional of the Cahn-Hilliard form, whereby they forgo the explicit description of discrete interactions and supersaturation of excess point defects and instead make use of effective interactions to account for the ballistic contributions. The model has been used to study compositional patterning in alloys driven by irradiation [14,16], phase stability of alloys under irradiation [13], nonequilibrium fluctuations in alloys under irradiation

*oforion@mcmaster.ca

[17], and irradiation-induced spinodal decomposition in the presence of dislocations [18]. The model can capture the appropriate long-time scales needed to examine sustained ballistic effects, but it does not incorporate different crystalline orientations, grain boundaries, defects, or elastoplastic effects. These are important in the microstructural and phase stability of NC materials under sustained external forcing.

In recent years, a new atomistic modeling paradigm coined the phase-field-crystal (PFC) method [19] has emerged. This approach is an effective modeling tool that describes microstructure evolution over diffusive time scales while incorporating atomistic-scale elasticity, topological defects, and grain boundaries. Several PFC models have been developed and used successfully in the description of solidification [20], spinodal decomposition [21], elastoplasticity [22], thin-film growth [23], and structural phase transformations in pure materials [24] and alloys [25]. The purpose of the present work is to incorporate the mesoscale model of ballistic effects in driven systems developed by Enrique and Bellon [14] into the PFC formalism to create a simulation framework capable of describing the evolution of composition and microstructure under ballistic conditions. Like the original model, the present model does not explicitly treat the supersaturation of point defects, and instead treats the long-time ensemble average of discrete ballistic effects through effective interactions. Our aim is to provide a modeling framework that is capable of simulating the long-time scales of sustained external forcing while incorporating the atomic effects mentioned previously. We will demonstrate the properties of the model by examining as a first example the grain growth behavior in the PFC formalism of NC materials under forced ballistic conditions.

The paper is organized as follows. First, we present the PFC model and its modification to account for ballistic effects. After introducing the model, we analyze the long-wavelength properties of the model, where we highlight modifications to the model of Enrique and Bellon. We follow with numerical simulations of grain growth under ballistic effects. Finally, we conclude and summarize.

II. EFFECTIVE PFC ENERGY FUNCTIONAL FOR BALLISTIC MIXING

We begin with the standard binary alloy PFC energy functional in scaled form [21],

$$\mathcal{F} = \int d\mathbf{r}\left\{\frac{n}{2}[B^{\ell} + B^{x}(2\nabla^2 + \nabla^4)]n - \frac{t}{3}n^3 + \frac{v}{4}n^4 + \frac{\omega}{2}\psi^2 + \frac{u}{4}\psi^4 + \frac{K}{2}|\vec{\nabla}\psi|^2\right\}, \tag{1}$$

where the energy is scaled by $k_B T\rho_{\ell} R^d$. The field n is the dimensionless local density, ψ is the dimensionless concentration, k_B is the Boltzmann constant, T is the temperature, ρ_{ℓ} is the reference liquid density, and R is the average atomic radius, with d being the dimensionality. Note the final three terms in Eq. (1) comprise a Cahn-Hilliard equation [26], which has been used to study phase separation. B^{ℓ} and B^{x} are the dimensionless bulk moduli of the liquid and solid, respectively, setting the energy scale of the system. Following Ref. [21], here we consider the lowest order expansion of the moduli where $B_{\ell} = B_0^{\ell} + B_2^{\ell}\psi^2$ and $B^{x} = B_0^{x}$. The remaining parameters are constants, which, in principle, are functions of the direct two-point correlation functions, and they can be calculated from first principles or fit to phenomenological databases or theories of material properties, e.g., surface energy [27–29]. However, the current work will only treat these parameters as constants. In the liquid phase, n is constant everywhere, while in the solid it assumes a spatially periodic structure. In two dimensions (2D), the functional in Eq. (1) has a phase diagram of coexisting liquid and solid phases with hexagonal symmetry. For greater detail in the derivation of the PFC energy functional presented in Eq. (1), the reader is referred to Ref. [21].

The density and concentration fields, n and ψ, follow dissipative dynamics that minimize $\mathcal{F}$. To include external forced ballistic effects, the dynamics are augmented by two Enrique and Bellon-like source terms in the density and concentration equations. They are written as

$$\frac{\partial n}{\partial t} = M\nabla^2\frac{\delta\mathcal{F}}{\delta n} - \Gamma\,(n - \langle n\rangle_{\mathcal{R}})\,, \tag{2}$$

$$\frac{\partial \psi}{\partial t} = M\nabla^2\frac{\delta\mathcal{F}}{\delta \psi} - \Gamma\,(\psi - \langle \psi\rangle_{\mathcal{R}})\,, \tag{3}$$

with M the mobility and Γ the frequency of forced atomic exchanges, proportional to the flux of incident particles. Note that Eqs. (2) and (3) are deterministic, however to incorporate the short-time fluctuations of the system, in Sec. IV when we report on numerical simulations, we append to these equations two stochastic variables, ζ and ξ, having a Gaussian distribution with zero mean and amplitudes A_{ζ} and A_{ξ} for the density and concentration fields, respectively. $\langle\,\psi\,\rangle_{\mathcal{R}}$ and $\langle\,n\,\rangle_{\mathcal{R}}$ denote the corresponding weighted spatial averages of the concentration and density fields, respectively, in response to forced atomic exchanges within an average distribution distance $\mathcal{R}$. The weighted averages are defined by

$$\langle\psi\rangle_{\mathcal{R}} = \int d\mathbf{r}' w_{\mathcal{R}}(\mathbf{r} - \mathbf{r}')\psi(\mathbf{r}') \tag{4}$$

and

$$\langle n\rangle_{\mathcal{R}} = \int d\mathbf{r}' w_{\mathcal{R}}(\mathbf{r} - \mathbf{r}')n(\mathbf{r}'). \tag{5}$$

The function $w_{\mathcal{R}}$ is a weight function describing the long-time spatial extent of ballistic exchanges in crystalline materials. A Yukawa potential was chosen as a form for the weight function in Ref. [14] for the case of exchanges driven by irradiation. However, in the present work we adopt the following 2D analog:

$$w_{\mathcal{R}}(r) = \frac{1}{2\pi\mathcal{R}^2}K_0\left(\frac{r}{\mathcal{R}}\right), \tag{6}$$

where K_0 is a modified Bessel function of the second kind. As stated above, $\mathcal{R}$ describes the average spatial extent of ballistic events and is also related to the energy of the ballistic driving force. We note that the above is the lowest-order description of ballistic events in driven systems that can be included for a binary alloy model that has coupling between density and composition variations. In general, Γ can take on different values for the density and concentration field, respectively, and two separate weight functions $w_{\mathcal{R}}^{n}$ and $w_{\mathcal{R}}^{\psi}$ can be introduced for each respective field. The model presented here, like the model

of Enrique and Bellon, has the underlying idea that a system exposed to external driving can be described by two mechanisms acting in parallel: thermal diffusion described by terms of the form $M\nabla^2\frac{\delta\mathcal{F}}{\delta n}$ and ballistic events described by terms of the form $\Gamma\,(n-\langle n\rangle_{\mathcal{R}})$. This is similar to the situation for the concentration order parameter. Note that when $\mathcal{R}=0$, the dynamics is driven only by the thermal portions of Eqs. (2) and (3).

Including only the lowest level of description, we construct an effective PFC energy functional for ballistic events, which affords an opportunity to explore equilibrium properties under ballistic conditions. Following Enrique and Bellon, we can write the effective functional as $E=\mathcal{F}+\gamma\mathfrak{G}$, where $\mathfrak{G}$ is the external energy representing effective interactions arising due to ballistic effects, and $\gamma=\Gamma/M$ is the reduced forcing frequency. The effective interactions are described by a self-interaction energy written as

$$\mathfrak{G}=\frac{1}{2}\int d\mathbf{r}\,d\mathbf{r}'\{n(\mathbf{r})g(\mathbf{r}-\mathbf{r}')n(\mathbf{r}')+\psi(\mathbf{r})g(\mathbf{r}-\mathbf{r}')\psi(\mathbf{r}')\}, \tag{7}$$

where the kernel for ballistic exchanges g satisfies the equation $\nabla^2 g(\mathbf{r}-\mathbf{r}')=-[\delta(\mathbf{r}-\mathbf{r}')-w_{\mathcal{R}}(\mathbf{r}-\mathbf{r}')]$. That is to say, the kernel satisfies the Poisson solution to a point source perturbed by a weight function.

III. LONG-WAVELENGTH AND EQUILIBRIUM PROPERTIES

We first interrogate the long-wavelength (i.e., phase-field) limit of the model. Secondly, we examine its bulk properties under forced driving, i.e., a kinetic phase diagram under ballistic conditions. To examine the long-wavelength properties of the model, we perform an amplitude expansion of our effective PFC free energy, E. To perform the expansion, we will be substituting into the effective free energy a single-mode expansion for the density,

$$n=n_o(\mathbf{r})+\sum_{\{\mathbf{G}_j,j\neq 0\}}\eta_j(\mathbf{r})e^{i\mathbf{G}_j\cdot\mathbf{r}}+\text{c.c.} \tag{8}$$

$n_o(\mathbf{r})$ is the dimensionless average density of the system, a conserved quantity which is slowly varying spatially with respect to the phase factors $\eta_j(\mathbf{r})$ are dimensionless spatially varying complex amplitudes which, like the average density, are slowly varying on atomic scales, $\mathbf{G}_j$ represents the lowest set of reciprocal basis vectors necessary to describe the crystal structure of interest, and c.c. denotes the complex conjugate. The result is then *coarse grained* using the volume averaging method of Refs. [28,29]. For a crystal of hexagonal symmetry in 2D, coarse graining E gives, to lowest order in the ballistic terms,

$$\begin{aligned}\tilde{E}=\int d\mathbf{r}\Bigg\{&\sum_{j=1}^{3}\left[\Delta B_0+\gamma\hat{g}(|\mathbf{G}_j|,\mathcal{R})+3\nu n_o^2-2tn_o\right]|\eta_j|^2+\sum_{j=1}^{3}\left[B_0^x|\mathcal{G}_j\,\eta_j|^2+\frac{3\nu}{2}|\eta_j|^4\right]+(6\nu n_o-2t)\left(\prod_{j=1}^{3}\eta_j+\text{c.c.}\right)\\&+6\nu\sum_{j,k>j}^{3}|\eta_j|^2|\eta_k|^2+\left(\omega+2B_2^{\ell}\sum_{j=1}^{3}|\eta_j|^2\right)\frac{\psi^2}{2}+\frac{u}{4}\psi^4+\frac{K}{2}|\vec{\nabla}\psi|^2+\left(\frac{\Delta B_0}{2}+\frac{B_2^{\ell}\psi^2}{4}\right)n_o^2-\frac{t}{3}n_o^3+\frac{\nu}{4}n_o^4\\&+\frac{B_0^x}{2}([1+\nabla^2]n_o)^2+\gamma\frac{n_o}{2}\int d\mathbf{r}'g(\mathbf{r}-\mathbf{r}')n_o(\mathbf{r}')+\gamma\frac{\psi}{2}\int d\mathbf{r}'g(\mathbf{r}-\mathbf{r}')\psi(\mathbf{r}')\Bigg\},\end{aligned} \tag{9}$$

where $\Delta B_0=B_0^{\ell}-B_0^x$ defines a temperature scale and the caret denotes the Fourier transform, with $\hat{g}=\mathcal{R}^2/(1+|\mathbf{G}_j|^2\mathcal{R}^2)$ and $\mathcal{G}_j\equiv\nabla^2+2i\mathbf{G}_j\cdot\nabla$. The free-energy functional of Eq. (9) describes a system with multiple crystal orientations, elastoplastic effects through the complex nature of the amplitudes, as well as density changes through the field n_o. Moreover, as a coarse-grained model, it operates on scales much larger than the lattice constant of the solid. A noteworthy result of Eq. (9) is that the $\gamma\hat{g}(|\mathbf{G}_j|,\mathcal{R})$ term competes with the temperature (ΔB_0), as both are modulated by the amplitude magnitude squared, $|\eta_j|^2$. In other words, forced external driving is manifested, partly, as shifts in the temperature scale leading to a new effective temperature. This is in agreement with previous theories of phase equilibria under driven conditions [5,15]. Furthermore, the ballistic term in concentration, $\gamma\frac{\psi}{2}\int d\mathbf{r}'g(\mathbf{r}-\mathbf{r}')\psi(\mathbf{r}')$, will be shown to renormalize the coefficient of the ψ^2 in the Cahn-Hilliard portion of the energy in the thermodynamic limit, i.e., the limit $\mathcal{R}\to\infty$. Namely, the model also predicts that ballistic effects cause alterations in the critical transition temperature as well. We also note that in the absence of density variations, defects, and the elastoplastic effects inherent in the complex nature of the amplitude formulation, i.e., all $|\eta_j|=$ const and scale out of the problem, we recover the Cahn-Hilliard ballistic model of Enrique and Bellon [14]. The repercussions of these effects are explored below when we construct phase diagrams for this model.

A. Pure material

The equilibrium phase diagrams follow standard minimization procedures analogous to Refs. [19,21]. For a pure material, we assume a real and constant amplitude $\eta_j\equiv\phi$ for all j and a constant wave vector to describe the periodicity of the solid, we ignore all terms in ψ, and we set $t=0$ and $\nu=1$. Making a long-wavelength approximation, i.e., $q\mathcal{R}\gg 1$, we first begin by minimizing the energy for the equilibrium wave vector, $q_{\text{eq}}=|\mathbf{G}_j|$, which is substituted back into the energy. Next, the energy is minimized for the real amplitude ϕ. After substitution of the minimized amplitude back into the energy,

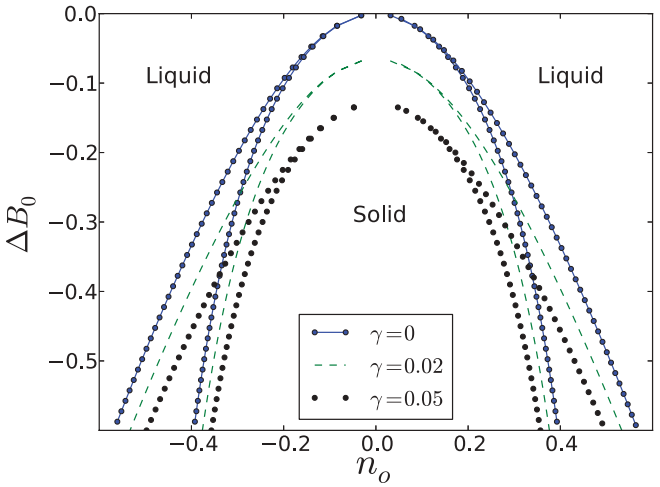

FIG. 1. (Color online) Kinetic phase diagram for a pure material exhibiting density variations in $\Delta B_0 \times n_o \times \gamma$ space, shown here projected onto the $\Delta B_0 \times n_o$ space for selected values of the reduced forcing frequency γ. Phase diagram plots the dimensionless temperature (ΔB_0) vs dimensionless average number density (n_o). Squares with lines (blue) represent the standard PFC model, $\gamma = 0$, dashed lines (green) correspond to a ballistic case of $\gamma = 0.02$, while squares (black) correspond to a ballistic case of $\gamma = 0.05$.

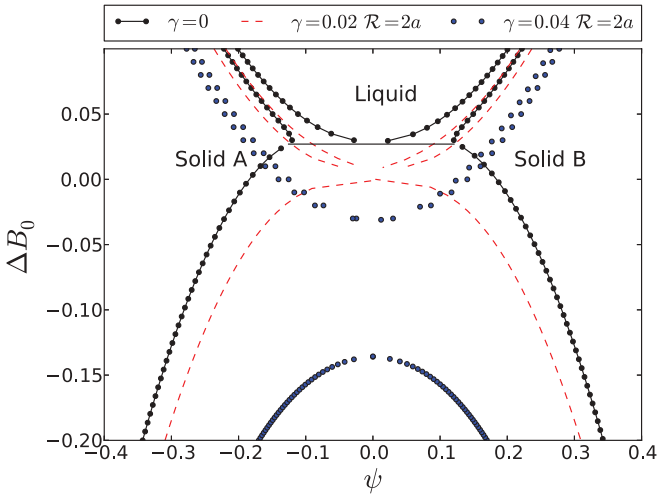

FIG. 2. (Color online) Binary eutectic phase diagram under forced ballistic driving. The kinetic phase diagram, here projected onto the $\Delta B_0 \times \psi$ phase space, plots the dimensionless temperature (ΔB_0) vs dimensionless concentration (ψ). Circles and lines (black) represent the standard binary PFC model, $\gamma = 0$, dashed lines (red) correspond to a ballistic case of $\gamma = 0.02$ and $\mathcal{R} = 2a$, while circles (blue) correspond to a ballistic case of $\gamma = 0.04$ and $\mathcal{R} = 2a$, with a being the lattice spacing.

we have a resulting energy which is a function of the conserved quantity n_o, temperature (ΔB_0), and the reduced forcing frequency γ. A common tangent or the equivalent Maxwell equal area construction leads to Fig. 1, which plots a dynamical phase diagram in ΔB_0, n_o, and γ space. We notice a trend of decreasing solid-liquid transition temperature with increasing γ. As previously discussed, we can attribute this behavior to the competition between the temperature and ballistic term, where in the thermodynamic, constant amplitude limit, the competition term takes the form $(\Delta B_0 + \gamma/q)\phi^2$.

B. Eutectic binary alloy

Moving on to the binary alloy, we again assume real and constant amplitude $\eta_j \equiv \phi$ for all j, and a constant wave vector q to describe the periodicity of the solid. We set $B_2^\ell = -1.8$, $B_0^x = 1$, $t = 0.6$, $\nu = 1$, $u = 4$, and $n_o = 0$. A spinodal and a eutectic alloy are differentiated, in this PFC model, by the choice of the parameter ω. Here we report the calculation for the eutectic alloy only, i.e., $\omega = 0.008$. After the parameters are set, we follow the same minimization steps as outlined for the pure material in the preceding section with respect to ϕ and $q_{\rm eq}$. With the average density being chosen to be zero, the resulting minimized energy is only a function of ψ, temperature (ΔB_0), reduced forcing frequency γ, and ballistic distance $\mathcal{R}$. A common tangent construction or equivalent Maxwell equal area construction gives Fig. 2. The figure presents the phase diagram of a eutectic alloy under ballistic effects in ΔB_0, ψ, and γ phase space. In the figure, $a = 2\pi/q_{\rm eq}$ is the lattice spacing associated with the hexagonal unit cell in 2D. There are several things to note. There is still a general shift of the solid-liquid transition temperature. Additionally, however, we also witness the alteration of the eutectic alloy into a spinodal alloy. Again, in the thermodynamic limit the coefficient of the amplitude square term becomes $(\Delta B_0 + \gamma/q)\phi^2$, which, from the pure material calculation above, was shown to affect the solid-liquid transition. This term is what primarily leads to the general shift in the solid-liquid transition. However, for the binary alloy, the coefficient multiplying the ψ^2 in the Cahn-Hilliard contribution becomes $(\omega + 12B_2^\ell\phi^2 + \gamma\mathcal{R}^2)\psi^2$. The $\gamma\mathcal{R}^2$ (i.e., $q\mathcal{R} \gg 1$) contribution to this term simultaneously accounts for the change from eutectic to spinodal, the increasing range of the solid solution region, and it contributes to the change in the solid-liquid transition lines in our model as well.

IV. DYNAMICS

Two sets of numerical simulations were conducted to study the role of ballistic driving on the grain growth of a pure nanocrystalline material. The first is designed to illustrate the physics of the proposed ballistic PFC term. The second set of simulations examines the grain growth behavior of a polycrystalline sample under ballistic conditions. For the simulations, we solve Eq. (2) with $\Delta x = 0.785$, $\Delta t = 1$, $M = 1$, $\Delta B_0 = -0.26$, $n_o = 0.285$, and $\zeta \neq 0$ (with amplitude $A_\zeta = 0.01$) using a semi-implicit Fourier technique.

A. Coarsening of a three-sided grain

For the first set of simulations, we have four grains as shown in the inset of Fig. 3 as an initial structure. In this configuration, conventional theory states that grains "1," "2," and "3" will tend to grow at the expense of grain "4," driven by gradients in the chemical potential resulting from curvature effects. Simulations were performed for the regular PFC dynamics ($\gamma = 0$) and for the proposed ballistic PFC model at $\gamma = 0.01$, with several values of the ballistic distance, i.e., $\mathcal{R} = 1a, 5a, 10a, 50a$, and $200a$. For a particular measure of

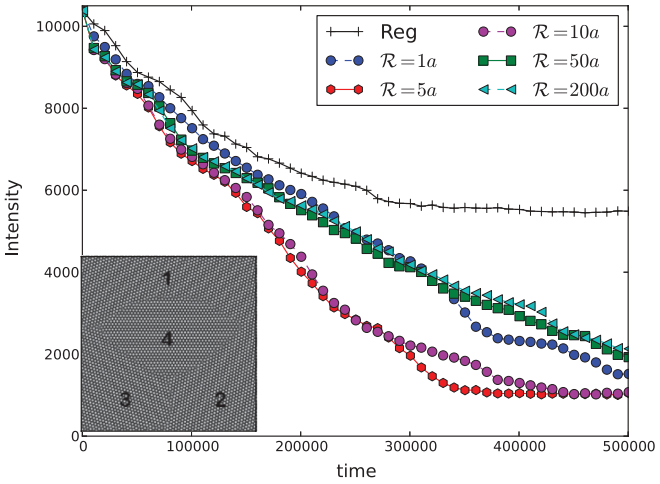

FIG. 3. (Color online) Grain intensity vs dimensionless time for $512\Delta x \times 512\Delta x$, with $\gamma = 0.01$ for varying $\mathcal{R}$. The left bottom inset shows an example of the initial microstructure used to perform the simulations. Density (n) map is shown, where lighter regions represent areas with a higher probability.

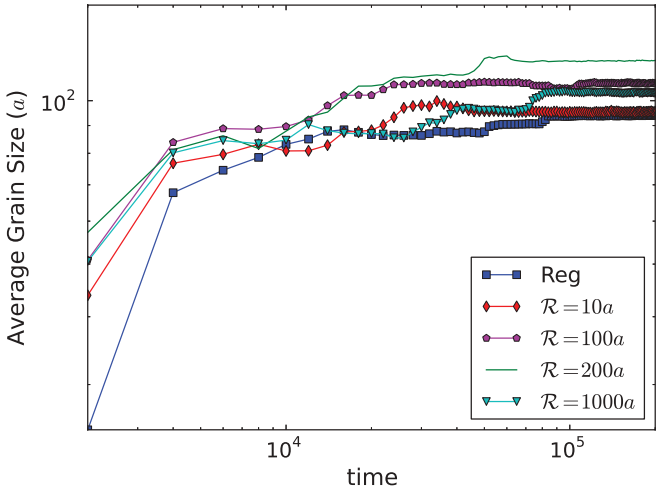

FIG. 4. (Color online) Grain growth results plotting average grain size vs time, on a log-log scale, for $1024\Delta x \times 1024\Delta x$. The grain size is a dimensionless quantity, measured in units of the lattice spacing, plotted against dimensionless time. Here $\gamma = 0.05$ for $\mathcal{R} = 10a$, $100a$, $200a$, and $\mathcal{R} = 1000a$.

the coarsening rate, we focus on the behavior of grain "4." Results were averaged over several runs, where grains "1," "2," and "3" assumed different orientations while keeping grain "4" fixed. In Fig. 3, we plot the average intensity of the Bragg peaks obtained from the power spectrum for grain "4" (which is proportional to its area) versus time. Several interesting aspects of the plot are noteworthy. First, the rate of coarsening is effectively enhanced for all cases of ballistic mixing. However, there exists two regimes of noteworthy behavior. Namely, we find one regime wherein the $\mathcal{R} = 5a$ and $10a$ conditions cluster and another for the $\mathcal{R} = 1a, 50a$, and $200a$ conditions. In the first regime, we have the fastest coarsening rates.

The results of Fig. 3 can be understood as follows. The long-time ballistic effect acts over a length scale $\mathcal{R}$, and within this spatial extent the mobility and/or driving force is enhanced. Thus, when $\mathcal{R}$ becomes comparable to the size of grain "4," the coarsening rate is more pronounced, as seen in the $\mathcal{R} = 5a$ and $10a$ cases. The plateaus evident at late time for these two conditions are a result of the background signal of the spectrum after the disappearance of grain "4" from the system. When the ballistic distance is much larger than the size of grain "4," i.e., $\mathcal{R} = 50a$ and $200a$ in the second regime, there is equal enhancement in the competition from all grains for growth (although still enhanced compared to the $\gamma = 0$ case). This results in a deadlock, which does not allow for preferential growth. Concerning $\mathcal{R} = 1a$, the spatial extent of this ballistic event is not large enough to impact any relevant length scales necessary for pronounced preferential growth. However, having an influence on all atomic length scales in the system, particularly those associated with boundary widths, it effectively behaves like the larger ballistic distances.

B. Grain growth

The second set of simulations examines grain growth for a nanocrystalline sample in a $1024\Delta x \times 1024\Delta x$ system, with approximately 100 grains. Figure 4 plots the average grain size versus time for $\gamma = 0.05$ for varying ballistic distances $\mathcal{R}$. Grain growth was quantified by Fourier analysis, where the full width at half-maximum of the Bragg peak was measured in the radially averaged signal. The multigrain simulations are consistent with the results of Fig. 3. Grain growth is enhanced for all $\mathcal{R}$ values. Also note that, in the time range of 500–1000, the average grain size is $75a$ and the growth is enhanced most strongly for $\mathcal{R}$ comparable to this grain size ($\mathcal{R} = 100a$). Therefore, our results demonstrate that nanocrystalline materials, although possibly offering increased resistance when exposed to ballistic driving forces, such as that from irradiation damage, are susceptible to enhanced grain growth under such driving forces, with the rate of growth generally increasing with increasing ballistic energy (i.e., $\mathcal{R}$), and they are particularly enhanced when $\mathcal{R}$ is comparable to the grain size.

V. SUMMARY AND CONCLUSIONS

In summary, we have developed an atomistic continuum model of competing effects between thermally activated diffusional processes and those driven by externally imposed ballistic events in both pure materials and alloys using a PFC free-energy functional. As an extension of the model of Enrique and Bellon, our approach is capable of describing defect microstructure, multiple crystal orientations, and elastoplastic effects. A long-wavelength analysis of our model predicts that ballistic events change the phase diagram through a shift in the solid-liquid transition temperatures for a pure material. For a eutectic alloy, the model further predicts an alteration of equilibrium through shifts in the critical transition temperatures in the solid solution regions, an effect which has long been conjectured in the irradiation damage literature. Through an investigation of the kinetic properties of the model, we find that under ballistic driving, grain growth is enhanced with increasing average ballistic distance,

with a predicted enhancement of grain sizes comparable to the ballistic range $\mathcal{R}$. Further numerical and experimental investigation is required to elucidate the possible myriad of behavioral aspects in a nanocrystalline system when subjected to ballistic driving.

ACKNOWLEDGMENTS

We acknowledge the National Science and Engineering Research Council of Canada (NSERC) for financial support, and David Montiel and Jonathan Stolle for useful discussions.

[1] G. Martin and P. Bellon, Solid State Phys. **50**, 189 (1997).
[2] K. Russell, Prog. Mater. Sci. **28**, 229 (1984).
[3] G. S. Was, Prog. Surf. Sci. **32**, 211 (1989).
[4] R. Cauvin and G. Martin, Phys. Rev. B **23**, 3322 (1981); **23**, 3333 (1981); **25**, 3385 (1982).
[5] F. Soisson, P. Bellon, and G. Martin, Phys. Rev. B **46**, 11332 (1992).
[6] S. M. Murphy, Europhys. Lett. **3**, 1267 (1987).
[7] Y. Limoge and A. Barbu, Phys. Rev. B **30**, 2212 (1984).
[8] X. M.-Bai, A. F. Voter, R. G. Hoagland, M. Nastasi, and B. P. Uberuaga, Science **327**, 1631 (2010).
[9] M. Rose, G. Gorzawski, G. Miehe, A. G. Balogh, and H. Hahn, Nanostruct. Mater. **6**, 731 (1995); M. Rose, A. G. Balogh, and H. Hahn, Nucl. Instrum. Methods Phys. Res., Sect. B **127-128**, 119 (1997).
[10] T. Hochbauer, A. Misra, K. Hattar, and R. G. Hoagland, J. Appl. Phys. **98**, 123516 (2005).
[11] M. J. Demkowicz, R. G. Hoagland, and J. P. Hirth, Phys. Rev. Lett. **100**, 136102 (2008).
[12] M. Samaras, P. M. Derlet, H. Van Swygenhoven, and M. Victoria, Phys. Rev. Lett. **88**, 125505 (2002); J. Nucl. Mater. **351**, 47 (2006).
[13] R. A. Enrique and P. Bellon, Phys. Rev. B **60**, 14649 (1999).
[14] R. A. Enrique and P. Bellon, Phys. Rev. Lett. **84**, 2885 (2000).
[15] G. Martin, Phys. Rev. B **30**, 1424 (1984).
[16] R. A. Enrique and P. Bellon, Phys. Rev. B **63**, 134111 (2001).
[17] R. A. Enrique and P. Bellon, Phys. Rev. B **70**, 224106 (2004).
[18] J. J. Hoyt and M. Haataja, Phys. Rev. B **83**, 174106 (2011).
[19] K. R. Elder, M. Katakowski, M. Haataja, and M. Grant, Phys. Rev. Lett. **88**, 245701 (2002).
[20] G. Tegze, L. Gránásy, G. I. Tóth, F. Podmaniczky, A. Jaatinen, T. Ala-Nissila, and T. Pusztai, Phys. Rev. Lett. **103**, 035702 (2009).
[21] K. R. Elder, N. Provatas, J. Berry, P. Stefanovic, and M. Grant, Phys. Rev. B **75**, 064107 (2007).
[22] P. Stefanovic, M. Haataja, and N. Provatas, Phys. Rev. Lett. **96**, 225504 (2006).
[23] Z.-F. Huang and K. R. Elder, Phys. Rev. Lett. **101**, 158701 (2008).
[24] M. Greenwood, N. Provatas, and J. Rottler, Phys. Rev. Lett. **105**, 045702 (2010); M. Greenwood, J. Rottler, and N. Provatas, Phys. Rev. E **83**, 031601 (2011).
[25] M. Greenwood, N. Ofori-Opoku, J. Rottler, and N. Provatas, Phys. Rev. B **84**, 064104 (2011).
[26] J. W. Cahn and J. E. Hilliard, J. Chem. Phys. **28**, 258 (1958); **31**, 688 (1959).
[27] K.-A. Wu and A. Karma, Phys. Rev. B **76**, 184107 (2007).
[28] S. Majaniemi and N. Provatas, Phys. Rev. E **79**, 011607 (2009).
[29] N. Provatas and S. Majaniemi, Phys. Rev. E **82**, 041601 (2010).